Transparent, High-Force, and High-Stiffness Control of Haptic Actuators with Backlash

Patrick Dills
Dept. of Mechanical Engineering
University of Wisconsin - Madison
Madison, United States
pdills@wisc.edu

Michael Zinn
Dept. of Mechanical Engineering
University of Wisconsin - Madison
Madison, United States
mzinn@wisc.edu

***Abstract*— Haptic actuators employing speed reductions display desirable increased force capability but have difficulty producing feelings of free space motion due to friction and inertia magnification implicit to actuator dynamics. This work describes a control topology that enables geared haptic actuators to produce highly transparent free space motion when combined with backlash nonlinearities. While the presence of backlash enables the proposed free space motion control, it is also a source of instability, limit cycles, and to some extent rendering distortion. We introduce a smoothed gain scheduling function to mitigate limit cycling and expand the range of stable impedances that can be rendered. The introduction of a design metric called the free space envelope provides a framework to evaluate the effectiveness of the free space controller. Together these two control approaches enable transparent free space, high-force, and stable haptic interactions in systems with backlash, a characteristic common in many speed reducers.**

Keywords—Backlash, Transparency, Stability, Haptic Actuators

I. Introduction

Kinesthetic haptic actuators must satisfy specific design requirements to function properly. Requirements for an interface, and consequently the actuators that compose it, can be summarized succinctly into three necessary criteria for an effective interface: Free space must feel free. (i.e., transparency), solid virtual objects must feel stiff. (i.e., stability), and virtual constraints must not be easily saturated [1].

Kinesthetic haptic actuation approaches can be generally categorized into impedance and admittance-controlled devices. Impedance-based designs are typically characterized by efficient low-reduction ratios. Low-reduction ratios (typically less than 10:1) facilitate transparent free space operation but limit the achievable rendering stiffness and high force rendering due to stability and actuator saturation constraints [1-3]. As speed reducer ratios increase, the torque capability of kinesthetic actuators linearly increases. However, the reflected inertia of the system increases with the reduction ratio squared. Increased inertia and damping from sizeable speed reducer ratios limit a device's ability to display free space motion.

Conversely, Admittance-based designs typically employ much larger gear ratios and consequently have much higher open-loop output impedances. Employing a high gear ratio allows these devices to display stiff high-impedance virtual constraints which are not easily saturated. Furthermore, closed-loop force control and an inner position control loop are used to reduce the system's output impedance for free space rendering. Unfortunately, stability and bandwidth restrictions of the force control loop limit an admittance control device's ability to mask its naturally high output impedance. Consequently, free-space rendering can feel less free as compared to impedance control approaches [4-6].

Other actuation approaches exist that can provide solutions to the problems inherent to impedance and admittance control approaches [7-10]. However, these approaches often employ redundant actuators, complicated designs, and complicated control approaches, which have hindered their widespread adoption.

In this work, we hope to address this need, through a novel control approach which allows highly geared actuators with backlash to achieve free space motion comparable to typical low-reduction devices like [1] and [2]. The larger gear reduction allows the actuator to display significantly higher forces and stiffness than typical impedance-controlled devices. To enable free-space transparency, we introduce a relative motion controller (see Fig. 1) that causes the motor to track the load position such that the gears are unloaded (or within the backlash gap) and decoupled from the load. This reduces the output impedance to that of the device's output dynamics alone (i.e. inertia and friction), improving free-space transparency. Furthermore, to mitigate common stability problems associated with backlash in position-controlled devices and impedance-based haptic devices [11,12] we introduce a gain scheduling control strategy which reduces the device's rendered impedance while the actuator is traversing the backlash gap (see Fig. 1). The control strategy enables high stiffness and high force rendering while avoiding limit-cycling that can occur when the gear train is unloaded (i.e. during load reversals). The controller switches between these two modes, relative motion control and gain scheduling control, to render free space and virtual environments. We find that the proposed approach enables convincing and accurate unilateral haptic environments common to kinesthetic haptic devices despite distortion introduced by backlash.

To facilitate the discussion of the proposed control approach, we first introduce a one-degree-of-freedom, nonlinear actuator model (section II). The control approach is discussed in two parts, first focusing on the free-space motion controller (section III), and then discussing the rendering control approach (section IV). The remainder of the paper includes an experimental evaluation (section V), and a short discussion of the control approaches limitations (section VI).

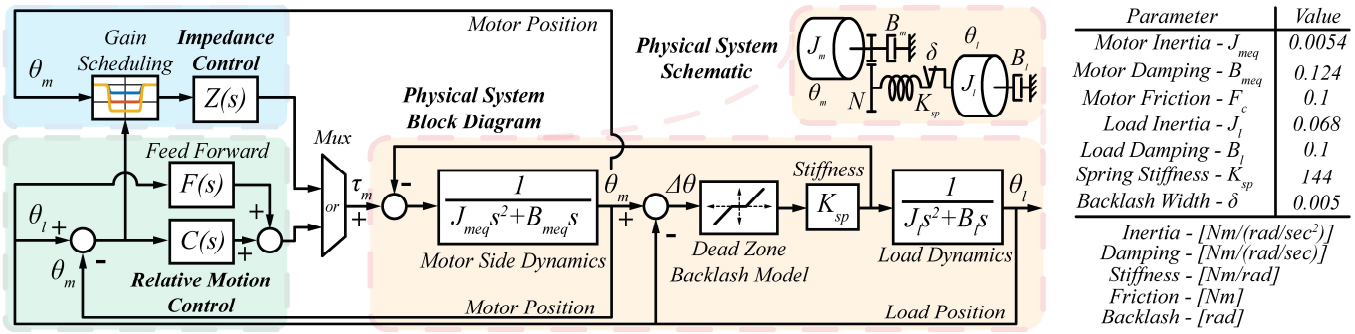

Parameter	Value
Motor Inertia - J_{meq}	0.0054
Motor Damping - B_{meq}	0.124
Motor Friction - F_c	0.1
Load Inertia - J_l	0.068
Load Damping - B_l	0.1
Spring Stiffness - K_{sp}	144
Backlash Width - δ	0.005

Inertia - [Nm/(rad/sec²)]
Damping - [Nm/(rad/sec)]
Stiffness - [Nm/rad]
Friction - [Nm]
Backlash - [rad]

Figure 1. A schematic, block diagram of the actuation approach, and parameter table. The mux indicates the "or" nature of the control approach. The relative motion controller is used to for free space rendering or the gain scheduled approach is used while rendering an impedance. Tabulated parameters are used for all calculations.

II. Single Degree of Freedom Model

A single degree of freedom model of our actuator is shown in Fig. 1. The physical actuator model is composed of an equivalent actuator side inertia and damping, a dead zone accounting for backlash, a relative stiffness representing the reducer's internal compliance, and a load inertia and damping. The model assumes both actuator and load position feedback. Additionally, time delays due to discretization or measurement latency are lumped into the impedance controller and the relative motion controller.

We model backlash with the commonly accepted dead zone [12]. The dead zone nonlinearity blocks any output over a range of inputs and prevents torque transfer between the motor and the load side within a small range of relative position amplitudes.

III. Free-Space Control Approach

As mentioned previously, a lack of transparency is likely the most significant obstacle to overcome when increasing an impedance-based haptic device's rendering capability through higher reduction ratios. A free space rendering control approach is necessary to enable the use of high-reduction actuators in haptics.

B. Relative Motion Control

Relative motion control exploits backlash to reduce the output impedance of our actuator. The relative motion controller, *C(s)*, and an optional feed-forward controller, *F(s)*, attempt to position the motor within the backlash dead zone (see Fig 1). The relative motion controller, *C*(*s*), typically could take the form of a proportional-derivative (*PD*) controller or lead compensator whereas the optional feed-forward control, *F*(*s*), could act directly on the desired acceleration. Relative motion control will prevent motor dynamics from being perceived on the load side where the user is coupled to the haptic device. Consequently, the device presents a high degree of free space transparency to the user, equal to that of the output link alone.

Our approach is somewhat comparable to the approach utilized by series elastic actuators in that it controls a relative deflection measurement [13]. However, the aim of our approach is to provide a zero torque mode instead of a torque source. Encountered type haptic displays utilize an analogous position tracking approach [14,15]. Other works employing similar control structures include [16] and [17] where relative position measurements have been recognized to induce a so-called "idling effect" which was used to improve force control. Additionally, relative position control has been shown to help damp flexible modes in position control applications [18].

C. The Free Space Envelope

While the free space motion controller described in the previous section can decouple the load from the drive train, to do so the finite dead-zone width (i.e. backlash) requires that the actuator track the load within this dead zone. Tracking errors that exceed the dead zone width will cause the actuator and load to make contact across the actuator's backlash and result in compromised free space motion.

To understand this effect, we define the *free space envelope*, as the frequency-dependent range of device position amplitudes over which the load side (i.e. device) dynamics remain isolated from the motor side dynamics. To derive the free space envelope we start with the equations of motion of the actuator dynamics.

$$\tau_m(t) = J_{meq}\ddot{\theta}_m(t) + B_{meq}\dot{\theta}_m(t) + N(A)K_{sp}\left(\theta_m(t) - \theta_l(t)\right) \quad (1)$$

$$0 = J_l\ddot{\theta}_l(t) + B_l\dot{\theta}_l(t) + N(A)K_{sp}\left(\theta_l(t) - \theta_m(t)\right) \quad (2)$$

Where $\tau_m(t)$ is the actuator torque input, J_{meq} is the equivalent actuator side inertia, and B_{meq} is the equivalent actuator damping. The dead zone nonlinearity, *N(A)*, can be considered a real-valued gain which varies between zero and one as a function of amplitude [19,20]. For amplitudes of oscillation below the backlash width *N(A)* remains zero and the final term of (1) can be eliminated. Taking the Laplace transform of (1), adding the feed-forward *F(s)* and relative motion control dynamics *C(s)* as shown in Fig. 1, and recognizing that the motor position θ_m can be rewritten in terms of the relative deflection $\Delta\theta$ and the load position θ_l leads to (3).

$$F(s)\theta_l(s) - C(s)\Delta\theta(s) = \left(J_{meq}s^2 + B_{meq}s\right)\left(\Delta\theta(s) + \theta_l(s)\right) \quad (3)$$

To form the transfer function $\theta_l(s)/\delta(s)$, we substitute backlash width δ in place of relative position, $\Delta\theta$, in recognition that this expression is valid only over finite oscillation amplitudes while the backlash gap is open (i.e. the backlash gap closes at oscillation amplitudes δ or greater). Rearranging and evaluating the magnitude yields an expression defining the free space envelope.

$$\left|\frac{\theta_l(s)}{\delta(s)}\right| = \left|\frac{J_{meq}s^2 + B_{meq}s + C(s)}{-\left(J_{meq}s^2 + B_{meq}s\right) + F(s)}\right| \quad (4)$$

Implementing proportional and derivative control as the relative motion controller (i.e. $C(s) = K_p + K_d s$) and neglecting

physical system damping, (B_{meq} = 0), and feed-forward control ($F(s)$ = 0) yields a free space envelope of the form (5). Normalizing by the motor inertia, J_{meq}, leads to the dimensionless expression in (6) where K_d is the derivative control gain, K_p is the proportional position control gain, ζ is the normalized damping ratio, and ω_n is the relative position controller's natural frequency.

$$\left|\frac{\theta_l(s)}{\delta(s)}\right| = \left|\frac{J_{meq}s^2 + K_d s + K_p}{-J_{meq}s^2}\right| \tag{5}$$

$$\left|\frac{\theta_l(s)}{\delta(s)}\right| = \left|\frac{s^2 + \frac{K_d}{J_{meq}}s + \frac{K_p}{J_{meq}}}{-s^2}\right| = \left|\frac{s^2 + 2\zeta\omega_n s + \omega_n^2}{-s^2}\right| \tag{6}$$

As seen in Fig. 2a, the free space envelope of an uncompensated system (i.e. open-loop system) has a normalized magnitude of one across all frequencies and is decoupled for oscillation amplitudes less than the backlash width. When a proportional-derivative (PD) relative motion controller is introduced, the free space envelope is widened, allowing for large amplitude low impedance free space motions, especially at low frequencies (Fig. 2a). The size of the free space envelope, as measured by the range of load oscillation amplitudes and frequencies over which the free space is increased, increases with the natural frequency, ω_n, and, thus, bandwidth of the relative motion controller. The relationship between controller gain and backlash width can be seen as a design tradeoff: higher gain allows for less backlash while larger backlash can accommodate a lower closed-loop bandwidth. It is also important to have a well-damped controller with minimal overshoot in its transient response, as an underdamped system can shrink the free space envelope around the system's natural frequency and reduce feelings of free space compared to the open-loop system.

In (6) we see that the proportional gain and the system's inertia determine the natural frequency and approximately determine the width and range of frequencies of the free space envelope. Feed-forward control acts on the system differently and decouples actuator dynamics directly. This effect can be seen by introducing inertial feed-forward control, $F(s) = J_{ff}s^2$, where the free space envelope becomes:

$$\left|\frac{\theta_l(s)}{\delta(s)}\right| = \left|\frac{J_{meq}s^2 + K_d s + K_p}{(J_{ff} - J_{meq})s^2}\right| \tag{7}$$

While ideal free space rendering is theoretically possible when $J_{ff} = J_{meq}$ (7), this is not achievable in practice given that perfect acceleration estimates are not available. Additionally, a second-order filter is necessary to make the feed-forward controller physically realizable. The filter prevents perfect free space rendering results from inertial feed-forward and limits the high-frequency effectiveness of feed-forward control. Note that over-estimation of inertia results in a decrease in the free space envelope's size compared to a perfectly estimated system. For example, in (7) if inertia is overestimated by a factor of two (i.e. J_{ff} = $2J_{meq}$) then the transfer function will have the same magnitude as the uncompensated system and free space rendering benefits from the feed-forward controller will be lost. Further increases beyond this estimated actuator inertia reduce the system's free space rendering capability compared to a system without inertial feed-forward.

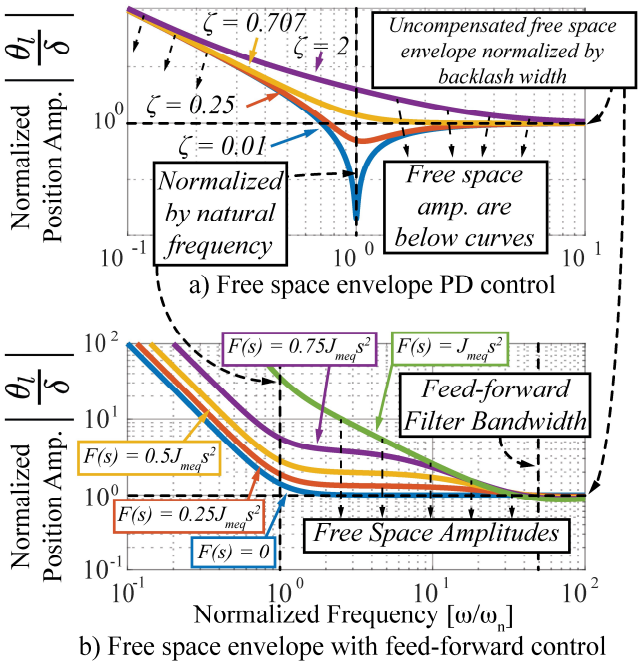

Figure 2. a) A normalized free space envelope considering PD control. The range of free space amplitudes is normalized by the backlash and the frequency is normalized by the system's natural frequency as defined in (6). b) The effect of an inertial feed-forward controller on the free space envelope. Curves also include a PD controller with a 0.707 damping ratio and a high frequency second order filter to make the feed forward control proper.

IV. Rendering Control

Impedance-controlled haptic devices render virtual impedances (such as a virtual wall) to users by measuring a device's position and commanding a device's force. When considering bilateral constraints, this rendering method is akin to a closed-loop position control system where the rendering impedance is equivalent to the controller's compensation (i.e. PD compensation). The magnitude of the rendering impedance (i.e. maximum stiffness or damping) is limited by the gain margin of the equivalent closed-loop system. In systems with low gear reductions and zero backlash, increasing the rendering gain, and thus decreasing the gain margin, can lead to oscillations and instability. In systems with large gear reductions and where backlash is present, limit cycling can occur as the rendering gain is increased [11,12].

A. Backlash-Induced Limit Cycles

Backlash induced limit cycles can be understood by separately considering the stability of the impedance control loop when the backlash gap is open (i.e. motor dynamics alone) and when the backlash gap is closed (i.e. rigidly connected load and motor dynamics). Specifically, the output inertia and damping of the system when the backlash gap is closed is much higher than when the actuator is traversing the backlash gap. This is especially true when a person is coupled to the output of a device. Increased inertia and damping result in an increased gain margin, which allows for a larger rendered impedance. Fig. 3 shows example Bode plots emphasizing the potential difference in stability margins while rendering a virtual stiffness. Instability resulting in limit cycling can be caused by increasing the virtual impedance to a value such that the actuator becomes unstable in the backlash gap.

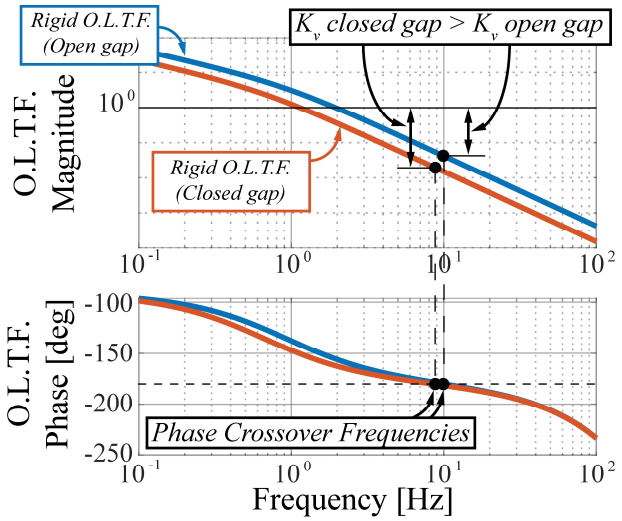

Figure 3. Bode plots of the open-loop transfer function showing how the system could be unstable when disconnected from the load (i.e. Open Gap) and stable when connected to the load (i.e. Closed Gap) for a stiffness.

B. *Limitations on Simplified Linear Limit Cycle Analysis*

As will be shown in Section V, where an experimental evaluation is discussed, the analysis of limit cycling per the reasoning of the previous section provides reasonable limit cycling predictions when the system time delay (due to sampling) is small. In systems with larger time delay, it is necessary to augment the analysis to include the effects of friction and compliance. We can simplify this analysis by recognizing that, when a human user is coupled to the driving point of the haptic device, the device remains stable over an increasing range of gains, in the sense that oscillations don't continually grow, while the disengaged system remains unstable. In this case, it is reasonable to assume that the output device is fixed (or locked) for the purposes of the limit cycling analysis. The augmented system dynamic model is shown in Fig 4. The equation of motion with a locked output is shown in (8).

$$\tau_m = J_{meq}\ddot{\theta}_m + B_{meq}\dot{\theta}_m + F_c sign(\dot{\theta}_m) + N(A)K_{sp}\theta_m \qquad (8)$$

Where the new variable F_c represents coulomb friction and $N(A)$ represents the backlash or dead zone dynamics.

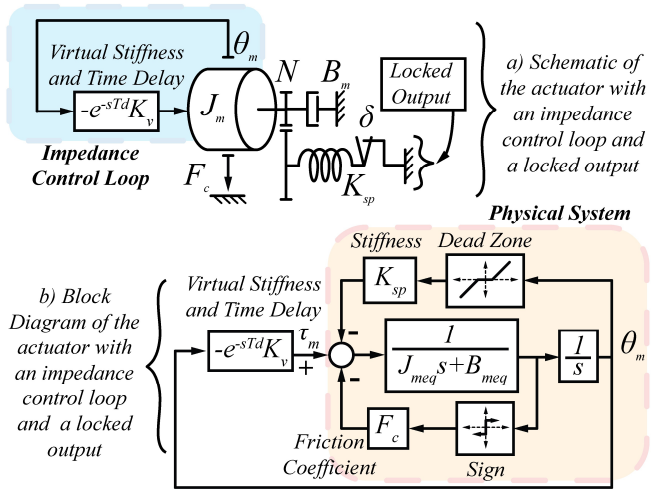

Figure 4. Simplified "Locked Output" models. A) Dynamic system model with impedance control loop, b) A simplified block diagram representation.

The describing function for coulomb friction and the dead zone nonlinearities are given in (9) and (10) respectively, where δ is the backlash or dead zone width and A is the assumed amplitude of motion, $\theta_m = A\sin(\omega t)$ [19,20].

$$N_{Fc}(t) = \frac{4F_c}{\pi\omega A} \qquad (9)$$

$$if\ A \le \delta \quad N(A) = 0$$
$$else \qquad (10)$$
$$N(A) = 1 - \frac{2}{\pi}sin^{-1}\left(\frac{\delta}{A}\right) - \frac{2\delta}{\pi A}\sqrt{1-\frac{\delta^2}{A^2}}$$

The two describing functions can be embedded in the equation of motion (8) and, with some manipulation, result in (11) which describes the open-loop dynamics of the locked system as a function of frequency and amplitude.

$$\frac{\theta_m(\omega)}{\theta_m(\omega)} = \frac{K_v e^{-j\omega T_d}}{\left(N(A)K_{sp} - J_{meq}\omega^2\right) + j\left(B_{meq}\omega + \frac{4F_c}{\pi A}\right)} \qquad (11)$$

We can treat (11) as the open-loop transfer function of the locked device rendering a virtual stiffness K_v and use it to evaluate stability, and thus the rendering limits of the system. As shown in Fig. 5, the magnitude of the open-loop transfer function varies with the assumed amplitude of oscillation, A. Fig. 5 shows that at high frequencies the system behaves almost identically to the simplified linear system presented in section IV-A. It is only at low frequencies that friction, backlash, and compliance begin to distort the system's open-loop frequency response. If we assume a system with large time delays the phase crossover frequency will occur where the magnitude frequency response is flat. Recognizing the DC content of the frequency response magnitude is maximized when the amplitude of oscillation is at the backlash width (i.e. the yellow dot in Fig. 5) allows us to develop an approximate symbolic expression for the maximum virtual stiffness before limit cycles are predicted (12).

$$1 = \left|\frac{K_{vMax}}{j\frac{4F_c}{\pi\delta}}\right| \rightarrow K_{vMax} \approx \frac{4F_c}{\pi\delta} \qquad (12)$$

This is done by setting the DC content (i.e. ω=0) of the open-loop transfer functions magnitude equal to one, assuming an amplitude of non-zero backlash width, δ (i.e $N(A) = 0$), and solving for virtual stiffness K_v.

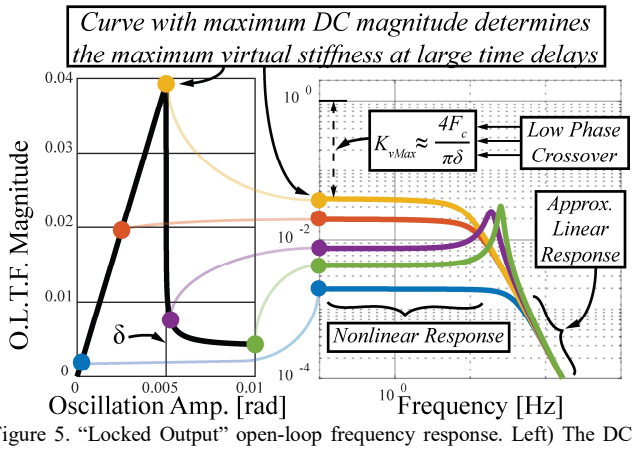

Figure 5. "Locked Output" open-loop frequency response. Left) The DC content of the FRF. Right) The effect of nonlinearities on magnitude. The virtual stiffness of the OLTF is K_v=1 such that (12) holds true.

Expression (12) provides a good approximation when the physical stiffness, K_{sp}, is much greater than K_{vMax} in (12) and time delays are large.

This analysis shows that at large time delays the limit cycling behavior of the system with backlash converges toward a constant virtual stiffness. If we solely relied on linear analysis from section III-A we would expect limit cycling to occur at decreasing virtual stiffness as time delay increases. Instead, the combination of friction and compliance causes the maximum virtual stiffness before limit cycling to saturate at approximately the value predicted by (12).

C. Gain Scheduling Control Strategy

As shown earlier in this section, the smaller inertia and damping of the system when it is traversing the backlash gap results in local instability and limit cycling. This observation motivates a gain scheduling (or rendering magnitude scheduling) approach, where the rendering magnitudes are reduced when traversing the backlash gap to maintain positive gain margin.

To implement the gain scheduling approach, we measure the relative motion of the system and detect if the system is traversing the backlash gap. To switch between controller gains we use the smoothed gain scheduling approximation in (13) and shown in Fig. 6.

$$f(\alpha, \beta, \Delta, \Delta\theta) = 1 - \alpha\left(\frac{1}{1+\left(\frac{\Delta\theta}{\Delta}\right)^{\beta}}\right) \tag{13}$$

In (13) β is an even-valued smoothing parameter that controls the transition between the high gain controller and the reduced gain controller. The gain reduction factor, α, is adjusted to eliminate limit cycling that occurs when traversing the backlash gap. The transition point, Δ, sets the value where the gain has changed by half its full-range value, and $\Delta\theta$ is the estimated relative deflection between the motor and load. Proper tuning of the gain scheduling approach requires measuring the actuator's backlash directly. The transition point, Δ, and the smoothing parameter, β, are adjusted to envelop the backlash gap. Subsequently, the gain reduction factor, α, reduces the gain in the backlash gap to achieve stable operation.

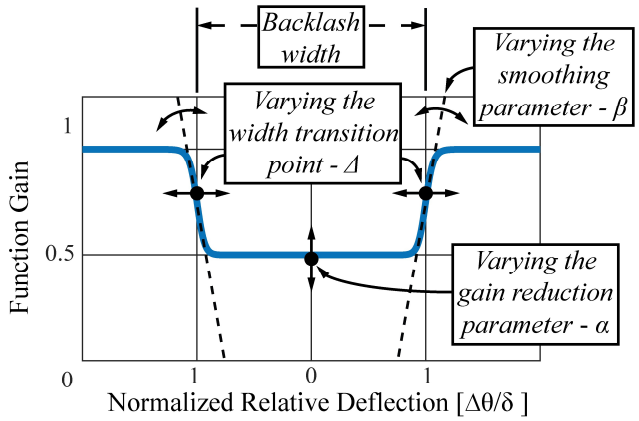

Figure 6. Impact of parameters on the smoothed gain scheduling function while varying the transition point, varying the smoothing factor, and varying the gain reduction factor.

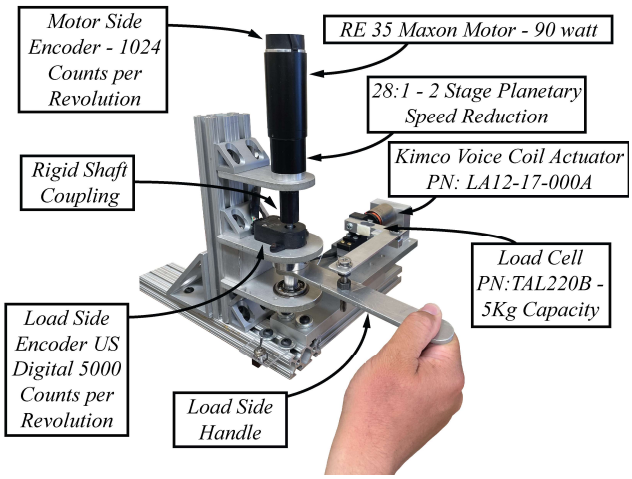

Figure 7. A one degree of freedom haptic actuation testbed and a voice coil and force sensor interface to provide disturbances to the system.

V. Experimental Evaluation

To investigate the control strategies presented here, we developed a one degree of freedom haptic interface (see Fig. 7). The actuator consists of a stock geared RE35 Maxon DC Motor (PN: 484753), with a 1024 count per revolution input encoder and a 28:1 two-stage planetary speed reducer. The motor is attached to the driving point handle of the haptic device with a rigid coupling to limit compliance. A US digital encoder (PN: E5-5000-375-IE-D-E-H-G-D) with 5000 counts per revolution measures the actuator's output position. Control methods run on a TI LAUNCHXL-F28069M development board operating at 1000 Hz sample frequency. The test stand also includes a Kimco linear voice coil actuator (PN: LA12-17-000A) and a strain gauge force sensor to measure interaction forces between the haptic actuator and the voice coil (PN: TAL220B-5Kg). Both the haptic actuator and voice coil are current-controlled with Copley Junus amplifiers (PN: JSP-090-10) and have an estimated current control bandwidth of 700 hertz.

A. Free Space Envelope Experimental Validation

The free space envelope defines the range of device output amplitudes and frequencies over which the actuator dynamics (i.e. motor inertia and damping) remain isolated from the output. Using the testbed described in the previous section, we experimentally validated its free space envelope by disturbing the system such that it narrowly remained within its free space envelope. The experiment was performed over a range of controller proportional gains, K_p. The voice coil actuator attached to the device's output supplied a disturbance consisting of a chirp signal from 1 to 50 hertz. The results are shown in Fig. 8. We found that a gain reduction of 50 percent was effective at mitigating limit cycles while maintaining the intended output impedance of the device. As shown in Fig. 8 increasing the proportional gain, K_p, increased the motion controller's bandwidth and natural frequency, resulting in an elevated low-frequency asymptote and an expanded free space envelope. For the specific device evaluated here the free space envelope was appreciably increased at a proportional gain of 70 [Nm/rad], resulting in approximately 0.45 rad of allowable output handle motion at 2 Hz as compared to the 0.005 rad of allowable motion from the backlash width alone.

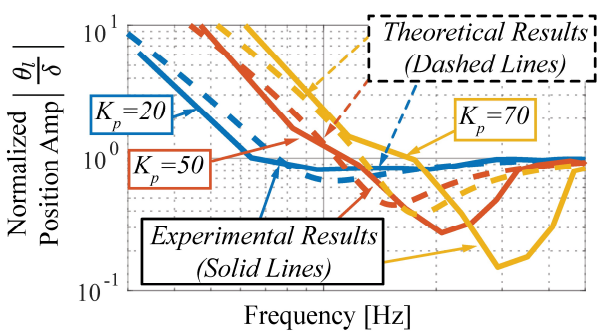

Figure. 8. The experimentally measured free space envelope for increasing proportional gains, K_p, compared to theoretical results. The frequency response function was constructed using a Hanning window, 50 percent overlap, and 400 frequency averages.

Proportional gains as high as 400 [Nm/rad] were implemented, resulting in a theoretically computed free space motions of approximately 2.35 rad at 2 Hz. These results were not included in Fig. 8 due to the limitations of the experimental validation setup (i.e. The input could not be forced to reach the backlash width at 2 hz). As the proportional gain is increased, the system's damping ratio is lowered. At higher values of proportional gain (K_p, = 70 [Nm/rad]), and without additional damping (i.e. K_d is kept constant), the controlled system becomes underdamped and the resulting resonance results in a reduced free space envelope in the vicinity of the controlled system's resonance frequency. At high frequencies (above the controller bandwidth) the motor can no longer effectively track the output position, causing the free space envelope magnitude to converge to one (i.e. equal to the backlash width). In this case, the load oscillations dominate the relative position output, forcing the free space envelope to converge to the backlash width. As shown in Fig. 8, the theoretically predicted free space envelope curves capture the experimental behavior. Deviations between theoretical and experimental results might be attributed to nonlinear friction in the gearhead.

B. *Stability and Limit Cycle Experimental Validation*

To validate the limit cycle analysis of Section V and explore the rendering performance of our proposed control approach, we experimentally evaluated the maximum achievable rendering stiffness. We measured the range of stable bilateral stiffness that our device can achieve under increasing time delays with a locked (or fixed) output (see Fig. 9). Limit cycling boundaries were experimentally determined by increasing the virtual stiffness and perturbing the system until a limit cycle was observed. The stiffness is subsequently decreased until the system stopped limit cycling. The stiffness where the limit cycle could no longer be sustained was considered the stability boundary in both the fixed output and human interaction test cases.

As seen in Fig. 9, the linear analysis from section IV-A predicts the limit cycling behavior well with a fixed device output and small time delays. However, for larger time delays the observed limit cycles deviate from the linear analysis. The numerical describing function analysis matches the experimental data across a wide range of time delays and converges toward the approximate analytical maximum stiffness (14) for large time delay values.

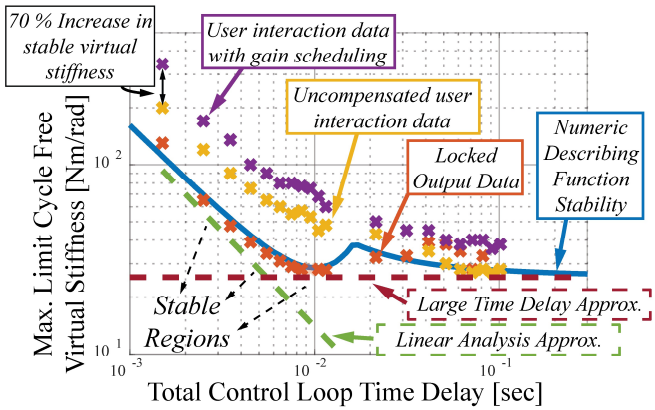

Figure. 9. The regions under the data represent regions of stable operation. Numerically predicted solid line from the describing function analysis. Gain scheduling parameters were set at β=30, Δ=0.007 rad, and α= 0.5

Additionally, we evaluated the onset of limit cycling behavior using the smoothed gain scheduling function described in section IV-C. The evaluation was performed while a user firmly gripped the device output. Results from this test show as much as a 70 percent increase in the limit cycle free range of stiffness as compared to the condition without the gain scheduling approach. We found that setting the transition point, Δ, slightly wider than the backlash width, δ, while using a large smoothing parameter (β=30) and a gain reduction, α, of 50 percent was effective at mitigating limit cycles while maintaining the intended output impedance of the device.

VI. Actuation Approach Limitations

While backlash and our control approach offer benefits, limitations still persist with regard to the output impedance of the device. Rendering distortion due to backlash occurs when the load and motor side are no longer connected. For virtual stiffness rendering, backlash-induced force artifacts manifest themselves under small output deflections. While not evaluated here, it is also likely that the distortion is more noticeable as the backlash width is increased and when using a bilateral stiffness constraint. Additional rendering distortion can result from the tuning of the gain scheduling parameters. For example, adjustment of the gain scheduling transition width, Δ, can result in lower perceived output impedance when it is set too large relative to the backlash width. When Δ is too small it could harm the controller's ability to suppress limit cycles. Additionally, the gain reduction in the backlash gap could allow users to perceive a lowered output impedance. In our experience, tuning the approach is easy in practice and rendering distortion is minimal.

VII. Conclusion, and Future Work

We have demonstrated a control approach that enables geared haptic actuators with backlash to produce highly transparent free space motion, high-force output, and high rendering stiffness. Future work should quantify and address rendering distortion along with extending the work to a multi-degree-of-freedom system.

VIII. Funding Statement

This work was supported by ONR grant No. N00014-22-1-2593, ONR Contract No. N00014-19-1-2023, NSF Grant 1830516, and the Madison Vilas Life Cycle Award.

References

[1] T. H. Massie and J. K. Salisbury. The phantom haptic interface: A device for probing virtual objects. In *Proceedings of the ASME Winter Annual Meeting, Symposium on Haptic Interfaces for Virtual Environment and Teleoperator Systems*, Chicago, IL, 1994. AMSE.

[2] S. Grange, F. Conti, P. Rouiller, P. Helmer, and C. Baur. Review of the delta haptic device. In *Proceedings of Eurohaptics 2001*, Birmingham, England, July 2001.

[3] J. E. Colgate and J. M. Brown, "Factors affecting the Z-Width of a haptic display," in *Proceedings of the 1994 IEEE International Conference on Robotics and Automation*, San Diego, CA, USA, 1994, pp. 3205–3210.

[4] R. V. der Linde, P. Lammertse, E. Frederiksen, and B. Ruiter. The hapticmaster, a new high-performance haptic interface. In *Proceedings of Eurohaptics 2002*, pages 1–5, Edinburgh, UK, 2002.

[5] A. Q. Keemink, H. van der Kooij, and A. H. Stienen, "Admittance control for physical human–robot interaction," *The International Journal of Robotics Research*, vol. 37, no. 11, pp. 1421–1444, Sep. 2018.

[6] C. Parthiban and M. Zinn, "Performance and stability limitations of admittance-based haptic interfaces," in *2018 IEEE Haptics Symposium (HAPTICS)*, San Francisco, CA, Mar. 2018, pp. 58–65.

[7] P. Dills, K. Gabardi, and M. Zinn, "Stability and Rendering Limitations of High-Performance Admittance Based Haptic Interfaces," in *2022 IEEE Haptics Symposium (HAPTICS)*, Santa Barbara, CA, USA, Mar. 2022, pp. 1–8.

[8] P. Dills, N. Colonnese, P. Agarwal, and M. Zinn, "A Hybrid Active-Passive Actuation and Control Approach for Kinesthetic Handheld Haptics," in *2020 IEEE Haptics Symposium (HAPTICS)*, Crystal City, VA, USA, Mar. 2020, pp. 690–697.

[9] M. Zinn, O. Khatib, B. Roth, and J. Salisbury. A new actuation approach for human friendly robot design. *Int. J. of Robotics Research*, 23(4/5):379–398, April-May 2002.

[10] C. Parthiban, P. Dills, I. Fufuengsin, N. Colonnese, P. Agarwal, and M. Zinn, "A Balanced Hybrid Active-Passive Actuation Approach for High-Performance Haptics," in 2019 IEEE World Haptics Conference (WHC), Tokyo, Japan, Jul. 2019, pp. 283–288.

[11] M. Nordin and P.-O. Gutman, "Nonlinear speed control of elastic systems with backlash," in *Proceedings of the 39th IEEE Conference on Decision and Control (Cat. No.00CH37187)*, Sydney, NSW, Australia, 2000, vol. 4, pp. 4060–4065.

[12] M. Nordin and P.-O. Gutman, "Controlling mechanical systems with backlash—a survey," Automatica, vol. 38, no. 10, pp. 1633–1649, Oct. 2002.

[13] Pratt, G.A., and M.M. Williamson. "Series Elastic Actuators." In *Proceedings 1995 IEEE/RSJ International Conference on Intelligent Robots and Systems. Human Robot Interaction and Cooperative Robots*, 1:399–406. Pittsburgh, PA, USA: IEEE Comput. Soc. Press, 1995.

[14] V. R. Mercado, M. Marchal and A. Lécuyer, ""Haptics On-Demand": A Survey on Encountered-Type Haptic Displays," in *IEEE Transactions on Haptics*, vol. 14, no. 3, pp. 449-464, 1 July-Sept. 2021.

[15] W. A. McNeely, "Robotic graphics: a new approach to force feedback for virtual reality," *Proceedings of IEEE Virtual Reality Annual International Symposium*, Seattle, WA, USA, 1993, pp. 336-341.

[16] S. Yamada and H. Fujimoto, "Proposal of high backdrivable control using load-side encoder and backlash," in *IECON 2016 - 42nd Annual Conference of the IEEE Industrial Electronics Society*, Florence, Italy, Oct. 2016, pp. 6429–6434.

[17] S. Yamada and H. Fujimoto, "Precise Joint Torque Control Method for Two-inertia System with Backlash Using Load-side Encoder," *IEEJ Journal IA*, vol. 8, no. 1, pp. 75–83, Jan. 2019.

[18] G. Ellis and R. D. Lorenz, "Resonant load control methods for industrial servo drives," in *Conference Record of the 2000 IEEE Industry Applications Conference. Thirty-Fifth IAS Annual Meeting and World Conference on Industrial Applications of Electrical Energy (Cat. No.00CH37129)*, Rome, Italy, 2000, vol. 3, pp. 1438–1445.

[19] J.-J. E. Slotine and W. Li, *Applied nonlinear control*. Englewood Cliffs, N.J: Prentice Hall, 1991.

[20] A. Gelb, *Multiple-input describing functions and nonlinear system design*. New York : McGraw-Hill, [1968], 1968.